Geophysical Research Letters

RESEARCH LETTER
10.1029/2019GL083623

Developing and Testing Physically Based Triggering Thresholds for Runoff-Generated Debris Flows

Hui Tang[1], Luke A. McGuire[1], Francis K. Rengers[2], Jason W. Kean[2], Dennis M. Staley[2], and Joel B. Smith[2]

[1]Department of Geosciences, University of Arizona, Tucson, AZ, USA, [2]U.S. Geological Survey, Golden, CO, USA

Key Points:
- Slope-dependent thresholds of dimensionless discharge and Shields stress can predict postfire debris flow initiation
- We propose a process-based method for calculating rainfall intensity-duration thresholds
- Rainfall intensity-duration thresholds derived from process-based hydrologic modeling are comparable to empirical thresholds

Supporting Information:
- Supporting Information S1

Correspondence to:
H. Tang,
huitang@email.arizona.edu

Citation:
Tang, H., McGuire, L. A., Rengers, F. K., Kean, J. W., Staley, D. M., & Smith, J. B. (2019). Developing and testing physically based triggering thresholds for runoff-generated debris flows. *Geophysical Research Letters*, *46*, 8830–8839. https://doi.org/10.1029/2019GL083623

Received 9 MAY 2019
Accepted 8 JUL 2019
Accepted article online 17 JUL 2019
Published online 5 AUG 2019

Abstract Runoff in steep channels is capable of transitioning into debris flows with hazardous implications for downstream communities and infrastructure, particularly in alpine landscapes with minimal vegetation and areas recently disturbed by wildfire. Here, we derive thresholds for the initiation of runoff-generated debris flows based on critical values of dimensionless discharge and Shields stress. These thresholds are derived by using a numerical model to estimate the hydrodynamic conditions coinciding with the timing of debris flow activity in a recently burned basin. A benefit of hydrodynamic thresholds is that they can be used to assess debris flow likelihood based on measurable hydrologic and geomorphic parameters and therefore provide more universal criteria for quantifying the runoff-to-debris flow transition in landscape evolution studies and hazard assessments. We then demonstrate how hydrodynamic thresholds can be used to estimate rainfall intensity-duration thresholds for runoff-generated debris flows without the need for historic debris flow observations.

1. Introduction

Runoff-generated debris flows are common in recently burned areas due to wildfire-induced effects on the soil and vegetation that substantially increase runoff and erosion relative to similar unburned areas (Moody et al., 2013). Many studies have demonstrated that postwildfire debris flows initiate once a critical rainfall intensity-duration (ID) threshold is exceeded (Staley et al., 2013, 2017). Rainfall ID thresholds are usually defined empirically for a given geographic region using historical data of debris flow occurrence and the triggering rainfall intensity (e.g., Bacchini & Zannoni, 2003; Bel et al., 2017; Caine, 1980; Cannon et al., 2008; Cannon et al., 2011; Destro et al., 2017; Giannecchini et al., 2016; Guo et al., 2016; Ma et al., 2017; Marra et al., 2016; Staley et al., 2013; Staley et al., 2015, 2017). However, direct observations and data constraining the precise timing of debris flow activity within rainstorms are rare (Bovis & Jakob, 1999), and it is difficult to accurately define rainfall ID thresholds when historical data are unavailable. Moreover, despite numerous studies focused on rainfall ID thresholds for postfire debris flows (Cannon et al., 2011; Staley et al., 2013, 2015, 2017), little is known about why rainfall thresholds vary from region to region or as a function of time since burning (Cannon et al., 2008).

We hypothesize that the hydrodynamic forces needed to initiate runoff-generated debris flows (in both burned and unburned terrain) are universal, but rainfall ID thresholds are variable in time and space because the transfer of rainfall to overland flow is largely regulated by regional differences in topography, vegetation, and soil infiltration properties. Laboratory experiments indicate that the initiation of runoff-generated debris flows can be related to hydrodynamic limits of dimensionless discharge (Gregoretti, 2000; Gregoretti & Fontana, 2008) and Shields stress (Prancevic et al., 2014). Gregoretti and Fontana (2008) suggest that runoff-generated debris flows initiate once a slope-dependent dimensionless discharge has been exceeded. They compared an experimentally derived dimensionless discharge threshold with estimated values of dimensionless discharge from debris flow producing storms in the Italian Dolomites, finding reasonable agreement between the two (Gregoretti & Fontana, 2008). More recently, Prancevic et al. (2014) conducted a series of laboratory flume experiments and found that a transition from bedload transport to en masse bed failure could be delineated by a slope-dependent, critical value of Shields stress. We test the applicability of these two metrics, dimensionless discharge and Sheilds stress, for predicting debris flow activity at the basin scale using a postfire debris flow dataset.

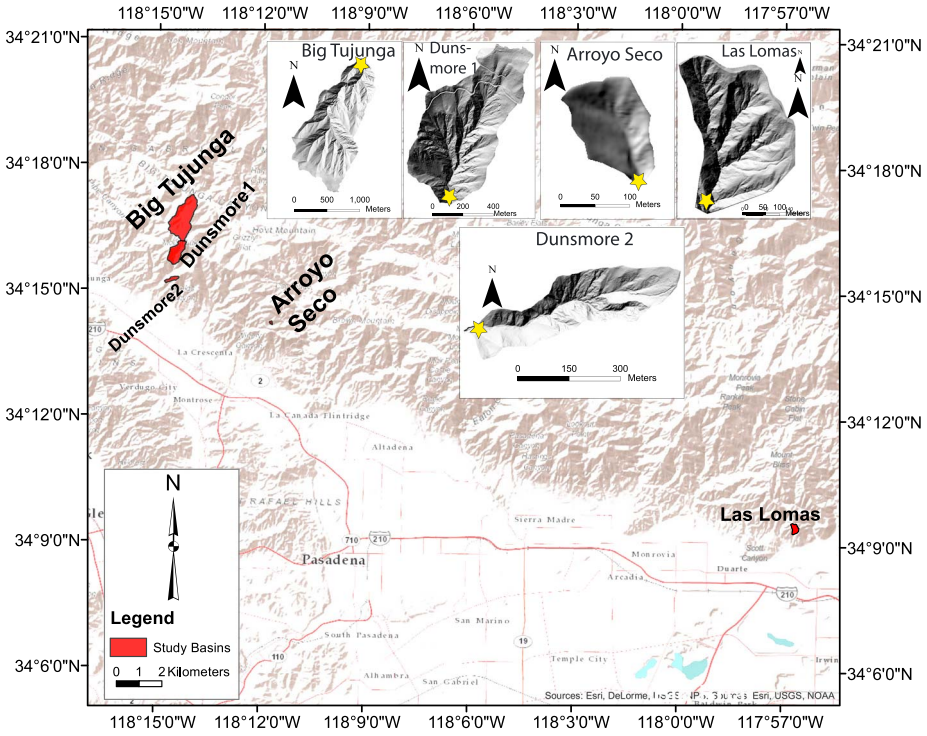

Figure 1. Shaded relief maps of the study areas in the San Gabriel Mountains: Big Tujunga, Las Lomas, Dunsmore 1, Arroyo Seco, and Dunsmore 2. Red areas indicate the study area. The yellow star marker on the shaded relief maps indicates the location of the stage gage at the outlet of each study site.

Using site observations from an intensively monitored burned area (Tang et al., 2019), we build on past work by testing the applicability of experimentally derived hydrodynamic thresholds for debris flow initiation in a natural setting. Specifically, we use a combination of numerical modeling and precise observations of debris flow timing in a basin burned by the 2016 Fish Fire in the San Gabriel Mountains to derive slope-dependent thresholds of dimensionless discharge and Shields stress to predict debris flow initiation. We then propose a method, given topography and an idealized rainstorm, to use the hydrodynamic thresholds and output from a hydrologic model to determine a rainfall ID threshold. Finally, we use this method to compute rainfall ID thresholds for four different basins in the San Gabriel Mountains. These four basins burned in the 2009 Station Fire (Kean et al., 2011) but have similar topography, lithology, climate, and vegetation as our study basin in the Fish Fire where the hydrodynamic thresholds are derived. The model-predicted rainfall ID thresholds are compared with existing regional ID thresholds derived through traditional empirical methods (Staley et al., 2013). A key benefit of using hydrodynamic criteria to develop debris flow initiation thresholds is that they can be used to derive rainfall ID thresholds in areas with no historical data on debris flow occurrence. Hydrodynamic criteria can also be more universally applied in other applications, including landscape evolution studies where it would be beneficial to quantify the potential for debris flow initiation in different portions of the drainage network.

2. Study Area

Our study sites include five watersheds in the San Gabriel Mountains, California, USA. First, we focus on deriving thresholds for runoff-generated debris flows using data from one watershed, referred to as Las Lomas, that was burned in the 2016 Fish Fire. Data from the four other nearby watersheds in the San Gabriel Mountains (Arroyo Seco, Dunsmore 1, Dunsmore 2, and Big Tujunga), which were burned during the 2009 Station Fire (Figure 1 and Table S1; Kean et al., 2011), are then used to conduct a series of simulations to test whether or not the proposed thresholds are consistent with empirically derived rainfall ID thresholds for the same region (i.e., the San Gabriel Mountains) that are known to be effective (Staley et al., 2013).

All five study basins have similar climate, vegetation, burn severity, and topographic characteristics (Figure 1 and Table S1). The climate in the San Gabriel Mountains is classified as Mediterranean, with relatively dry

summers and wet winters. Chaparral is the dominant vegetation community. The study basins have average slopes that vary from 46° to 51° (Kean et al., 2011; Tang et al., 2019). Soils are typically sandy, but hillslopes also have a gravel component of >20% (Kean et al., 2011; Tang et al., 2019). Soil depths range from roughly 0.5 to 1 m (Kean et al., 2011; Tang et al., 2019).

Digital elevation models (DEMs) derived from airborne lidar with a 1-m resolution were available for the Big Tujunga, Dunsmore 1, and Dunsmore 2 basins (Heimsath et al., 2019). The DEM for the watershed at Las Lomas (3-m resolution) was also derived from airborne lidar (Kean et al., 2019; Tang et al., 2019). For the Arroyo Seco watershed, a 1-m DEM was produced from terrestrial laser scanner survey data (Staley et al., 2014). All postfire debris flows in these study sites were generated by runoff (Kean et al., 2011; Tang et al., 2019), in contrast to unburned settings where debris flows are often mobilized from rainfall-induced shallow landslides (e.g., Iverson et al., 1997).

3. Methodology

3.1. Monitoring Debris Flow Activity at Las Lomas

Threshold values of dimensionless discharge and Shields stress are derived here by using a numerical model to reconstruct the hydrologic conditions throughout the Las Lomas watershed at times leading up to observed debris flow activity. The first step in this process is to identify the timing of debris flow activity within rainstorms. We monitored debris flow activity at the outlet of the Las Lomas watershed following the 2016 Fish Fire and identified seven rainstorms during the first postfire year that produced runoff (Kean et al., 2019; Tang et al., 2019). Two of the rainstorms resulted only in water-dominated flows (Figure S2 and Table S2). The other five rainstorms produced debris flows, generating 11 periods of debris flow activity within those storms.

Monitoring equipment deployed at Las Lomas included a disdrometer and a tipping bucket rain gauge, both of which were used to quantify rainfall intensity, as well as a channel monitoring station near the basin outlet that included two geophones, a rain-triggered video camera, and a laser distance meter to measure stage (Figure 1; Kean et al., 2019). The channel monitoring station is similar to that used by Kean et al. (2011, 2016). We identified the onset of debris flow activity at the channel monitoring station using ground velocities recorded by the geophones (e.g., Kean et al., 2015), which increase rapidly during the passage of debris flow surges (e.g., Arattano & Marchi, 2005; Suwa et al., 2009), and from stage data where debris flows produce asymmetric shapes in the hydrograph (an abrupt rise in stage followed by a slow decline; Kean et al., 2011). Water-dominated flood peaks were identified in the stage data as broader peaks with more symmetric shapes (Kean et al., 2011). When storms occurred during daylight hours, video imagery was also used to confirm the presence of debris flow (Kean et al., 2019; Tang et al., 2019). Additional details regarding debris flow monitoring and the postfire hydrogeomorphic response to different storms can be found in Kean et al. (2019) and Tang et al. (2019).

3.2. Numerical Model

We simulate fluid flow and sediment transport throughout our study sites, including both channel and hillslope areas, using the model developed by McGuire et al. (2016, 2017), which has been previously applied to simulate postwildfire runoff and sediment transport processes in the San Gabriel Mountains. Rainfall-runoff and sediment transport processes are modeled by combining the two-dimensional, nonlinear shallow water equations with a set of advection equations to track the movement of sediment in different particle size classes. Infiltration is simulated using the Green-Ampt equation, which requires knowledge of the saturated hydraulic conductivity (K_s) and wetting front capillary pressure head (h_f; Green & Ampt, 1911). The Hairsine-Rose (HR) soil erosion model is used to simulate sediment detachment and transport processes (Hairsine & Rose, 1991, 1992a, 1992b). The model also accounts for channel bed failure processes, which may be caused by the formation and subsequent failure of temporary sediment dams (e.g., Kean et al., 2013) and can lead to rapid increases in local sediment concentration (McGuire et al., 2017). When sediment concentrations are less than 20%, flow resistance is determined using a depth-dependent Manning coefficient (Jain et al., 2005). The equations governing fluid motion include an additional resistance term associated with debris flow, based on a Coulomb friction law where the effective basal normal stress is modified by pore-fluid pressure (e.g., Iverson & Denlinger, 2001), that begins to influence flow dynamics once sediment concentration exceeds 20% and becomes progressively more impactful as sediment concentration increases (Jain et al., 2005; McGuire et al., 2016).

Runoff and sediment transport parameters were constrained for the Las Lomas watershed through a combination of field measurements and model calibration (see Tang et al., 2019, for a complete description of the model setup). The hydraulic roughness parameter (a depth-dependent Manning coefficient) was calibrated for each rainstorm based on a comparison between modeled and measured stage (Figure S1). Sediment transport parameters needed for the HR soil erosion model at Las Lomas, including two parameters related to the detachability of sediment by raindrop impact and one parameter that represents the detachability of sediment by flow-driven processes, were calibrated by comparing modeled hillslope erosion to maps of hillslope erosion derived from multitemporal terrestrial laser scanner surveys (McGuire & Rengers, 2019; Tang et al., 2019). Infiltration parameters needed for the Green-Ampt infiltration model (K_s and h_f) were determined from field measurements made using a mini disk tension infiltrometer (Kean et al., 2019; Tang et al., 2019). Particles size classes for the sediment transport model are based on grain size analyses from the hillslopes and from dry ravel deposits within the channel, as detailed by Tang et al. (2019).

Comparisons between modeled and recorded stage at the basin outlet are presented in Figure S1 for the seven runoff-producing rainstorms, and supporting information Table S1 contains a summary of hydrologic model parameter values used in simulations for each study basin. Simulations at Big Tujunga, Dunsmore 1, and Dunsmore 2 are performed using a runoff-only version of the model with parameters calibrated by Rengers et al. (2016). Sediment transport is not included in these three cases since we lack the data required to constrain model parameters related to sediment transport at those sites. Model parameters used for simulations at Arroyo Seco, including those needed to simulate sediment transport, are based on a model calibration performed by McGuire et al. (2016). We assess and discuss the impact of using a runoff-only model compared to a model that includes both sediment transport and runoff processes in section 4, and a sensitivity analysis is presented in the supporting information (Figures S6 and S7).

3.3. Deriving Physically Based Thresholds for Debris Flow Initiation

Runoff and sediment transport are simulated for each of the seven runoff-generating rainstorms at Las Lomas, which allowed us to compute the dimensionless discharge and Shields stress as a function of time for every channel location in the basin. In particular, we are interested in quantifying typical values of dimensionless discharge and Shields stress at (1) times when debris flows are initiating and (2) times when there is a flood response that does not include any debris flow activity. Similar to Parker et al. (1982) and Gregoretti and Fontana (2008), we calculate the dimensionless discharge as

$$q_* = \frac{q}{\sqrt{\frac{\rho_s-\rho}{\rho} g D_{50}^3}}, \tag{1}$$

where $q = h\sqrt{u^2+v^2}$ is discharge, h represents water depth, u and v denote velocity in x and y directions, D_{50} is the median grain size, ρ and ρ_s are the density of water and sediment respectively, and g is gravity acceleration. Here, we constrain D_{50} based on particle size analyses from the matrix of debris flow deposits at each of our study sites (Table S1). The Shields stress is calculated by

$$\tau_* = \frac{\tau}{(\rho_s-\rho) g D_{50}}, \tag{2}$$

where $\tau = \rho g h S_f$ is shear stress with $S_f = n_0^2(uh^2+vh^2)h^{-10/3}$ being the friction slope and n_0 denoting Manning's roughness coefficient.

Since we are interested in the values of q_* and τ_* within debris flow initiation areas at the times when debris flows are initiating, we compute time-averaged values of q_* and τ_* within the channel network over a 10-min window of time before the known passage of debris flows at the basin outlet. More specifically, 10-min averages of q_* and τ_* from throughout the channel network are binned by the slope to obtain an approximation for typical values for q_* and τ_* as a function of slope within the channel network. Data are binned by slope since past experiments suggest that debris flow initiation thresholds based on either q_* or τ_* are slope dependent (Gregoretti & Fontana, 2008; Prancevic et al., 2014). We compute time-averaged values of q_* and τ_* rather than instantaneous values since the precise time of debris flow initiation is unknown. Only the time at which debris flows exit the watershed is known. In rainstorms where a debris flow did not occur, we quantify q_* and τ_* within the channel network during a 10-min time window leading up to the time of peak flow at the outlet. In section 5, we discuss how averaging q_* or τ_* over different time intervals influences results and explain the selection of a 10-min time interval.

Letting t_{pass} denote the time at which a debris flow passes by the basin outlet, we define $q_{*,T}(S) = q_*(S, t_{pass} - T \leq t \leq t_{pass})$ as the time average of dimensionless discharge prior to the time of debris flow detection at the basin outlet. Unless otherwise noted, $T = 10$ denotes the time in minutes before the debris flow passes by the basin outlet. Similarly, $\tau_{*,T}(S) = \tau_*(S, t_{pass} - T \leq t \leq t_{pass})$. Note that both $q_{*,T}(S)$ and $\tau_{*,T}(S)$ are functions of slope (S). Debris flows will take some time to travel from their initiation points to the outlet, meaning that if we were to limit our analysis to using $q_*(S, t = t_{pass})$ and $\tau_*(S, t = t_{pass})$, then we would undoubtedly be examining the hydrodynamic conditions occurring after debris flow initiation. Unless noted otherwise, we use q_* and τ_* in the remainder of the manuscript to denote $q_{*,10}(S)$ and $\tau_{*,10}(S)$, respectively.

A conservative estimate of the dimensionless discharge threshold for debris flow initiation can be estimated as the lowest value of q_* during a debris flow producing storm. We refer to this threshold as the lower limit (LL) for debris flow initiation, following the terminology adopted by Cannon et al. (2008). A less conservative estimate of the dimensionless discharge threshold for debris flow initiation can be defined by taking the average of q_*, for a given slope, from all of the debris flow producing storms. We refer to this threshold as the upper limit (UL). We define the upper limit (UL) and lower limit (LL) thresholds for Shields stress analogously with one modification. We could not use the lowest value of τ_*, for a given slope, during a debris flow producing storm to define the Shields stress LL threshold due to the overlap between τ_* associated with debris flow events and τ_* associated with water-dominated responses. Instead, the LL threshold for Shields stress is defined as the average τ_*, for a given slope, during all water-dominated floods.

3.4. Estimating Rainfall ID Thresholds From Hydrodynamic Thresholds

The physically based thresholds for dimensionless discharge and Shields stress are used to estimate rainfall ID thresholds. This is accomplished by simulating the runoff response from idealized rainstorms and comparing the predicted values of q_* and τ_* to the newly developed thresholds. For example, we determine whether or not an average intensity of I mm/hr for a duration of D minutes is above or below the ID threshold by simulating the runoff response to a rainstorm that lasts D minutes and has an average intensity of I mm/hr. Rainfall intensity is spatially uniform and time dependent with a normal distribution (Figure S5). If the physically based threshold for debris flow initiation is exceeded during the design rainstorm, then we assume the rainfall ID threshold has also been exceeded. In cases where sediment transport is included in the model formulation, such as at Arroyo Seco, the UL thresholds are used; otherwise, the LL thresholds are applied, with the assumption that a runoff-only model will tend to underpredict flow depth and discharge relative to a model that includes the bulking effects of sediment. Since thresholds based on dimensionless discharge or Shields stress are a function of slope, which is binned in increments of 1° from 10° to 45°, the criteria for exceeding the physically based threshold is an exceedance of the critical value within more than half of the slope bins. The idealized rainstorms have durations of 15, 30, and 60 min and average rainfall intensities ranging from 5 to 40 mm/hr (in increments of 1 mm/hr, see Figure S5). Based on the results of these simulations at each of the five study basins, we can determine basin-specific rainfall ID thresholds that can be compared with the regional ID thresholds derived for the San Gabriel Mountains using historical data (e.g., Staley et al., 2013).

4. Results

4.1. Physical Thresholds

Simulations of runoff and sediment transport at the Las Lomas watershed demonstrate that q_* is greater during debris flow producing storms relative to storms that only produce water-dominated flows (Figure 2). Both the LL and UL dimensionless discharge thresholds derived here are greater than thresholds proposed by Gregoretti (2000) and Tognacca et al., 2000 (2000; Figure 2c). In order to summarize the general relationship between q_* and slope suggested by our numerical experiments, we note that the LL and UL thresholds for q_* can be fit to curves with the same form as those proposed by Gregoretti and Fontana (2008):

$$q_* = \frac{C}{[\tan(\theta)]^N} \tag{3}$$

where θ is the slope angle. Best fit coefficients for the UL threshold are $C = 12.0$ and $N = 0.85$ while they are $C = 4.29$ and $N = 0.78$ for the LL threshold.

Typical values of Shields stress during times of debris flow initiation are high compared with Shields stress thresholds for bed failure obtained from flume experiments (Prancevic et al., 2014) and derived theoretically

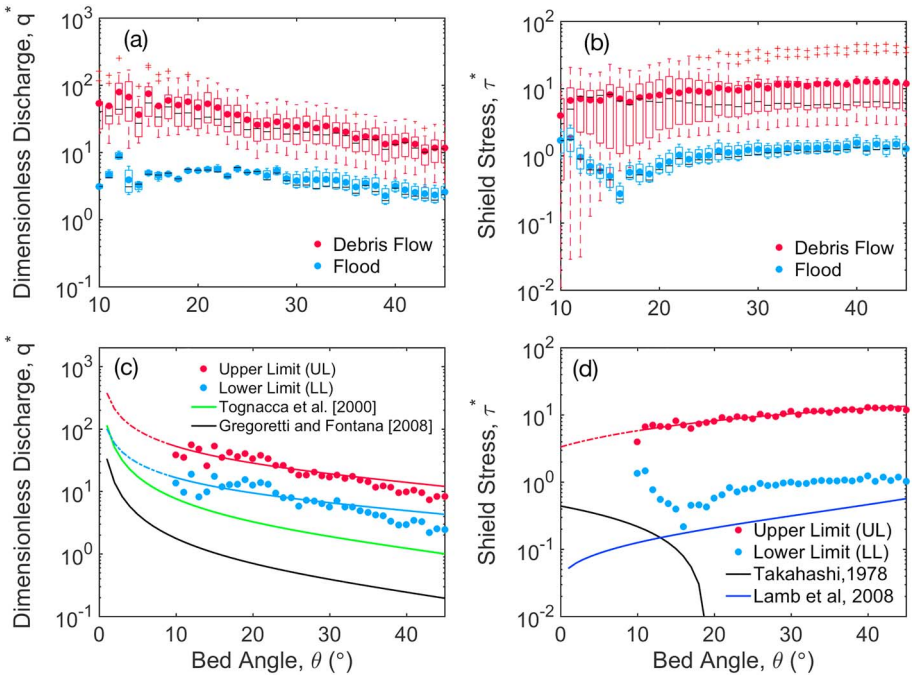

Figure 2. Hydrodynamic thresholds derived from simulations at Las Lomas: (a) Dimensionless discharge (q_*) and (b) Shields stress (τ_*) at Las Lomas as a function of slope. Red dots with range represent binned values over the 10-min interval prior to debris flow arrival at the lower monitoring station. Blue dots with range represent dimensionless discharge during water-dominated events (i.e., no debris flows) in the 10 min leading up to the time of peak flow depth at the lower station. (c) Comparison between the upper limit q_* threshold (UL, red dots and fit curve, red line), lower limit q_* threshold (LL, blue dots and fit curve, blue line), and the thresholds proposed by Tognacca et al. (2000) and Gregoretti and Fontana (2008). (d) Comparison between the upper limit τ_* threshold (UL, red dots and fit curve) and lower limit τ_* threshold (LL, blue dots) with experimental data quantifying thresholds for incipient sediment motion (Lamb et al., 2008) and the onset of bed failure (Prancevic et al., 2014; Takahashi, 1978) given the measured friction angle of 34° (Tang et al., 2019).

by Takahashi, (1978; Figure 2d). The UL threshold for τ_* can be approximated well by a function of the form

$$q_* = p_1 * \theta^2 + p_2 * \theta + p_3. \quad (4)$$

where $p_1 = -0.00067$, $p_2 = 0.25$, and $p_3 = 3.32$. However, the LL Shields stress threshold is nonmonotonic and not fit well by a single function (Figure 2d).

4.2. Rainfall Intensity-Duration Thresholds

The UL and LL thresholds for q_* and τ_* derived at Las Lomas were applied to estimate rainfall ID thresholds at durations of 15, 30, and 60 min for the four watersheds (Arroyo Seco, Dunsmore 1, Dunsmore 2, and Big Tujunga) burned by the 2009 Station Fire. The UL thresholds are applied in Arroyo Seco; the LL thresholds are used for rest of basins. For reference, empirical rainfall ID thresholds for the San Gabriel Mountains are 19, 13, and 12 mm/hr for durations of 15, 30 and 60 min, respectively (Staley et al., 2013). Using the threshold based on dimensionless discharge, we derive 30-min rainfall thresholds of 16 mm/hr (Arroyo Seco), 15 mm/hr (Dunsmore 1), 14 mm/hr (Dunsmore 2), and 13 mm/hr (Big Tujunga), which are close to the empirically derived regional threshold (13 mm/hr; see Figure 3). On average, the percent difference between the regional threshold and rainfall thresholds derived from q_* are 17%, 8%, and 14% for durations of 15, 30, and 60 min, respectively. Rainfall thresholds derived from the Shield stress threshold deviate from the regional thresholds by 20%, 8%, and 10% for durations of 15, 30, and 60 min, respectively (Figure 3). A model sensitivity analysis using the data from Arroyo Seco indicates that uncertainties of ±50% in the value of hydrologic variables, namely, saturated hydraulic conductivity and hydraulic roughness, lead to uncertainties in the predicted rainfall ID thresholds of approximately 2–3 mm/hr (Figure S7).

In general, rainfall thresholds derived from q_* and τ_* are greater than the regional threshold for 15-min durations and less than the regional threshold for 60-min durations. One potential explanation for this trend is

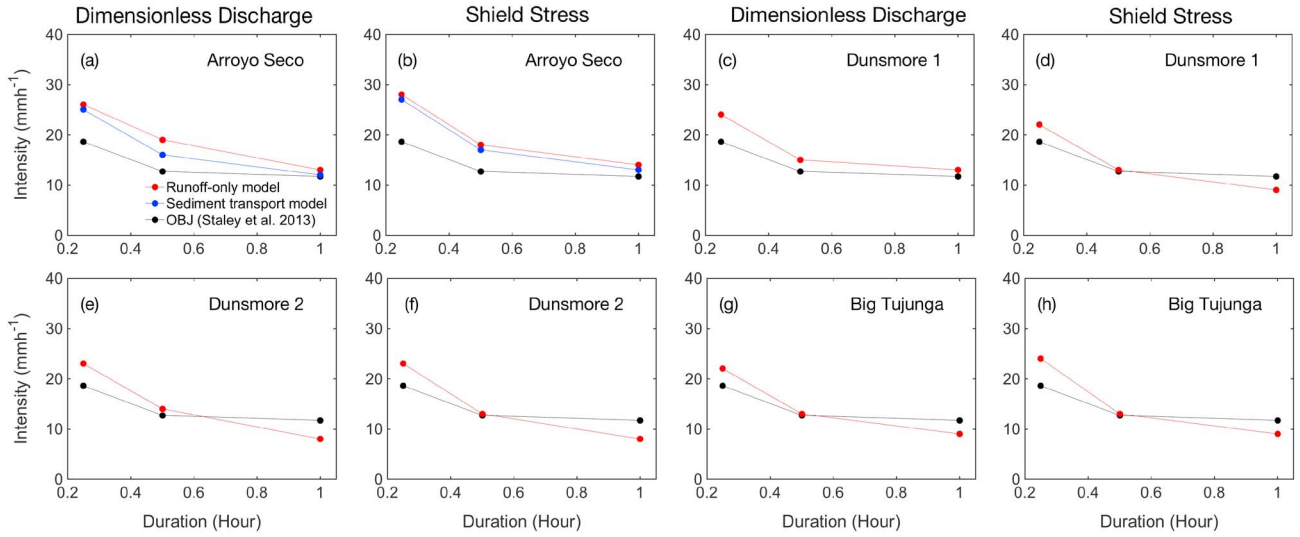

Figure 3. Comparison of rainfall intensity-duration (ID) thresholds based on dimensionless discharge (a, c, e, and g) or Shields stress (b, d, f, and h) and regional rainfall ID thresholds (OBJ) for Arroyo Seco (a and b), Dunsmore 1 (c and d), Dunsmore 2 (e and f), and Big Tujunga (g and h) in San Gabriel Mountains, California, USA. The black line represents the objectively defined rainfall ID thresholds derived by Staley et al. (2013). Blue circles represent rainfall ID thresholds derived from simulations using a coupled model for runoff and sediment transport. Red dots represent rainfall ID thresholds derived from simulations with a runoff-only model.

that we use idealized storms with rainfall intensity time series that have a Gaussian shape (Figure S5) in order to connect the q_* and τ_* thresholds with a rainfall threshold. In reality, however, the within-storm distribution of natural rainfall is complex and will also play a role in determining the runoff response. Oakley et al. (2017) found that a particular combination of atmospheric conditions, including atmospheric rivers, are generally present when postfire debris flows are triggered in the Transverse Ranges of Southern California. Therefore, the types of rainstorms that tend to produce the intense rainfall that triggers debris flows may share particular characteristics (e.g., in terms of variability of rainfall intensity and storm cumulative rainfall). Utilizing idealized rainstorms that are designed to represent the temporal variations present in natural rainfall within a local region may result in improved estimates of rainfall ID thresholds.

5. Discussion

Results demonstrate that dimensionless discharge and Shields stress are generally greater during the 10-min time period leading up to observed debris flows compared with the 10-min time period leading up to the passage of a water-dominated flood (Figure 2). Both the LL and UL thresholds for dimensionless discharge that were obtained in our study watershed are greater than the thresholds for dimensionless discharge suggested by Tognacca et al. (2000) and Gregoretti and Fontana (2008). Moreover, there are large differences between the Shields stress threshold derived here and the criteria suggested by Takahashi (1978) and determined experimentally by Prancevic et al. (2014). The LL and UL Shields stress thresholds are well above the bed failure threshold predicted by Prancevic et al. (2014) and Takahashi (1978) at high slopes and lie within the sheet flow regime defined by Palucis et al. (2018). As a consequence, the criteria proposed by Prancevic et al. (2014) and Takahashi (1978) may lead to underestimates of the amount of rainfall required to produce debris flows within a given drainage basin. The apparent discrepancy between thresholds derived here and those derived previously may arise from the fact that previous studies have focused on a threshold at which the bed fails (Prancevic et al., 2014) or at which rapid scouring occurs in a thin layer of sediment (Gregoretti, 2000). It is unclear whether or not bed failure will result in a debris flow since that will depend on the amount of sediment eroded and the resulting concentration of that sediment in the water column following entrainment. Postwildfire environments, including our study area, are also generally characterized by an abundance of fine-grained sediment which may further complicate direct comparisons between our analyses and the experiments from Gregoretti (2000) and Prancevic et al. (2014), which were conducted with gravel. More generally, the particle size distribution of the sediment that was involved in the debris flow initiation process, which we constrain from the matrix of debris flow deposits, introduces an element of uncertainty in the calculations of q^* and τ^*. Note, however, that dry ravel from hillslopes left thick,

cohesionless deposits that blanketed most of the channel network, where debris flows were likely to be initiating, during the first several postfire rainstorms at Las Lomas (Tang et al., 2019). Particle size analysis from a dry ravel deposit within the steep, upper portion of the channel network at Las Lomas revealed a D_{50} of 0.8 mm which is similar to the D_{50} of 0.63 mm obtained from a debris flow deposit near the basin outlet.

The choice to average values of dimensionless discharge and Shields stress over a 10-min time window is based on past observations in the Transverse Ranges of Southern California that debris flows typically reach the basin outlet of small watersheds (0.01–1 km^2) within 5–10 min of intense rainfall (Kean et al., 2012). Simulations indicate that there is only a small amount of separation between values of $\tau_{*,1}(S)$ (i.e., 1-min averages) associated with debris flow events and values of $\tau_{*,1}(S)$ associated with water-dominated floods at Las Lomas (see supporting information Figure S4). This may result from the fact that debris flows likely initiate several minutes before they reach the outlet and therefore averaging over a 1-min interval may not be sufficiently long to capture the hydrologic conditions that lead to initiation. In contrast, averaging q_* and τ_* over 25 min leads to separation of debris flows and the water-dominated floods (see supporting information Figures S3 and S4). However, 25 min is substantially longer than observed debris flow response times for the small watersheds (0.01–1 km^2) considered here (Kean et al., 2012). Averaging q_* and τ_* over time periods from 5 or 10 min appears reasonable and produces similar results (Figure S3 and S4). An additional consideration is if it is necessary to include sediment transport in the simulations to predict rainfall ID thresholds from hydrodynamic criteria. Our results show that rainfall ID thresholds derived from the runoff-only model are slightly larger than those estimated using a model that accounts for sediment transport (Figures 3 and S6). The primary reason is that the discharge of postwildfire runoff can increase due to the addition of debris (e.g., Kean et al., 2016). However, applying the LL threshold for dimensionless discharge or Shields stress in conjunction with runoff-only simulations potentially compensates for these underestimations. This result is encouraging since sediment transport parameters may be poorly constrained in many applications.

An additional benefit of establishing hydrodynamic thresholds for debris flow initiation is that, unlike rainfall ID thresholds, hydrodynamic thresholds should not vary based on the hydrologic properties of the landscape. For example, soil hydraulic properties, hydraulic roughness, and rainfall interception change with time following wildfire (Ebel & Moody, 2017; Moody et al., 2013, 2016; Nyman et al., 2014; Stoof et al., 2012) and influence the rainfall-runoff processes that affect runoff-generated debris flows. Rainfall ID thresholds for debris flow initiation will therefore change with time (e.g., Cannon et al., 2008), but thresholds based on dimensionless discharge and Shields stress will remain constant. Therefore, given data that constrains how hydrologic input variables change as a function of time since burning, the thresholds derived here for dimensionless discharge and Shields stress can be applied to determine how rainfall ID thresholds change with time and can be used to identify the wildfire-induced hydrologic changes that have the most impact on debris flow potential. The applicability of both rainfall ID thresholds and hydrodynamic thresholds, however, is based on the assumption that there is sufficient sediment available to generate a debris flow.

Although hydrodynamic thresholds afford increased versatility relative to rainfall ID thresholds, there are two reasons that we propose a method to estimate rainfall ID thresholds using hydrodynamic criteria. First, there may not always be sufficient time in operational scenarios to apply a physically based model. Second, the utility of empirical rainfall ID thresholds is well established in the San Gabriel Mountains (e.g., Staley et al., 2013). The hydrodynamic thresholds developed here should be broadly consistent with previously published rainfall ID thresholds for the study region (Figure 3). Simulations of idealized rainstorms with different durations and intensities demonstrate that this is indeed the case for four different basins in the San Gabriel Mountains. The proposed method for generating rainfall ID thresholds based on hydrodynamic criteria provides a promising alternative to empirical methods for assessing the potential of runoff-generated debris flows.

6. Conclusion

In this study, we derived critical thresholds for the initiation of postwildfire debris flows based on slope-dependent values of dimensionless discharge and Shields stress. Further, we present a method for estimating rainfall ID thresholds using a processes-based hydrologic model and the proposed physically based thresholds. Rainfall ID thresholds derived from the proposed method produce estimates that compare well with established empirical rainfall ID thresholds for the San Gabriel Mountains. Results establish

a new method to estimate rainfall ID thresholds in areas where there is little or no observational record of debris flow occurrence. The physically based debris flow initiation thresholds derived here also make it possible to incorporate the effects of changing hydrologic conditions on debris flow initiation, which could be particularly valuable in addressing debris flow hazards within recovering burn areas.

Acknowledgments
We thank the Editor Harihar Rajaram, one anonymous reviewer, and Brian McArdell for helpful comments that improved the quality of the manuscript. This work was partially supported by the U.S. Geological Survey (USGS) Landslide Hazards Program. Any use of trade, product, or firm names in this paper is for descriptive purposes only and does not constitute endorsement by the U.S. Geological Survey. The code for the numerical model is stored in the Community Surface Dynamics Modeling System (CSDMS) model repository at the website (https://csdms.colorado.edu/wiki/Model:SWEHR). Data used in this manuscript are stored in the USGS ScienceBase archive at https://doi.org/10.5066/P92HVD2T, https://doi.org/10.5066/P9F3YTBP, and OpenTopography at 10.5069/G94M92N4.

References

Arattano, M., & Marchi, L. (2005). Measurements of debris flow velocity through cross-correlation of instrumentation data. *Natural Hazards and Earth System Science*, *5*(1), 137–142.

Bacchini, M., & Zannoni, A. (2003). Relations between rainfall and triggering of debris-flow: Case study of Cancia (Dolomites, Northeastern Italy). *Natural Hazards and Earth System Sciences*, *3*(1/2), 71–79. https://doi.org/10.5194/nhess-3-71-2003

Bel, C., Liebault, F, Navratil, O., Eckert, N., Bellot, H., Fontaine, F., & Laigle, D. (2017). Rainfall control of debris-flow triggering in the Real Torrent, Southern French Prealps. *Geomorphology*, *291*, 17–32. https://doi.org/10.1016/j.geomorph.2016.04.004

Bovis, M. J., & Jakob, M. (1999). The role of debris supply conditions in predicting debris flow activity. *Earth Surface Processes and Landforms*, *24*(11), 1039–1054. https://doi.org/10.1002/(SICI)1096-9837(199910)24:11<1039::AID-ESP29>3.0.CO;2-U

Caine, N. (1980). The rainfall intensity-duration control of shallow landslides and debris flows. *Geografiska Annaler: Series A, Physical Geography*, *62*(1-2), 23–27. https://doi.org/10.1080/04353676.1980.11879996

Cannon, S. H., Boldt, E. M., Laber, J. L., Kean, J. W., & Staley, D. M. (2011). Rainfall intensity–duration thresholds for postfire debris-flow emergency-response planning. *Natural Hazards*, *59*(1), 209–236. https://doi.org/10.1007/s11069-011-9747-2

Cannon, S. H., Gartner, J. E., Wilson, R. C., Bowers, J. C., & Laber, J. L. (2008). Storm rainfall conditions for floods and debris flows from recently burned areas in southwestern Colorado and Southern California. *Geomorphology*, *96*(3), 250–269. https://doi.org/10.1016/j.geomorph.2007.03.019

Destro, E., Marra, F., Nikolopoulos, E. I., Zoccatelli, D., Creutin, J. D., & Borga, M. (2017). Spatial estimation of debris flows-triggering rainfall and its dependence on rainfall return period. *Geomorphology*, *278*, 269–279. https://doi.org/10.1016/j.geomorph.2016.11.019

Ebel, B. A., & Moody, J. A. (2017). Synthesis of soil-hydraulic properties and infiltration timescales in wildfire-affected soils. *Hydrological Processes*, *31*(2), 324–340. https://doi.org/10.1002/hyp.10998, hYP-16-0392.R1

Giannecchini, R., Galanti, Y., Avanzi, G. D., & Barsanti, M. (2016). Probabilistic rainfall thresholds for triggering debris flows in a human-modified landscape. *Geomorphology*, *257*, 94–107. https://doi.org/10.1016/j.geomorph.2015.12.012

Green, H. W., & Ampt, G. (1911). The flow of air and water through soils. *Journal of Agriculture Science*, *4*(1), 1–24.

Gregoretti, C. (2000). The initiation of debris flow at high slopes: Experimental results. *Journal of Hydraulic Research*, *38*(2), 83–88. https://doi.org/10.1080/00221680009498343

Gregoretti, C., & Fontana, G. D. (2008). The triggering of debris flow due to channel-bed failure in some alpine headwater basins of the Dolomites: Analyses of critical runoff. *Hydrological Processes*, *22*(13), 2248–2263. https://doi.org/10.1002/hyp.6821

Guo, X., Cui, P., Li, Y., Ma, L., Ge, Y., & Mahoney, W. B. (2016). Intensity-duration threshold of rainfall-triggered debris flows in the Wenchuan earthquake affected area, China. *Geomorphology*, *253*, 208–216. https://doi.org/10.1016/j.geomorph.2015.10.009

Hairsine, P. B., & Rose, C. W. (1991). Rainfall detachment and deposition: Sediment transport in the absence of flow-driven processes. *Soil Science Society of America journal*, *55*(2), 320–324.

Hairsine, P. B., & Rose, C. W. (1992a). Modeling water erosion due to overland flow using physical principles: 1. Sheet flow. *Water Resources Research*, *28*(1), 237–243. https://doi.org/10.1029/91WR02380

Hairsine, P. B., & Rose, C. W. (1992b). Modeling water erosion due to overland flow using physical principles: 2. Rill flow. *Water Resources Research*, *28*(1), 245–250. https://doi.org/10.1029/91WR02381

Heimsath, Arjun., Whipple, Kelin., Lamb, Michael., & Hudnut, K. (2019). Mapping of San Gabriel Mountains, CA 2009 Fire, National Center for Airborne Laser Mapping (NCALM), distributed by OpenTopography. https://doi.org/10.5069/G94M92N4

Iverson, R. M., & Denlinger, R. P. (2001). Flow of variably fluidized granular masses across three-dimensional terrain: 1. Coulomb mixture theory. *Journal of Geophysical Research*, *106*(B1), 537–552. https://doi.org/10.1029/2000JB900329

Iverson, R. M., Reid, M. E., & LaHusen, R. G. (1997). Debris-flow mobilization from landslides. *Annual Review of Earth and Planetary Sciences*, *25*(1), 85–138. https://doi.org/10.1146/annurev.earth.25.1.85

Jain, M. K., Kothyari, U. C., & Raju, K. G. (2005). GIS based distributed model for soil erosion and rate of sediment outflow from catchments. *Journal of Hydraulic Engineering*, *131*(9), 755–769. https://doi.org/10.1061/(ASCE)0733-9429(2005)131:9(755)

Kean, J. W., Coe, J. A., Coviello, V., Smith, J. B., McCoy, S. W., & Arattano, M. (2015). Estimating rates of debris flow entrainment from ground vibrations. *Geophysical Research Letters*, *42*, 6365–6372. https://doi.org/10.1002/2015GL064811

Kean, J. W., McCoy, S. W., Tucker, G. E., Staley, D. M., & Coe, J. A. (2013). Runoff-generated debris flows: Observations and modeling of surge initiation, magnitude, and frequency. *Journal of Geophysical Research: Earth Surface*, *118*, 2190–2207. https://doi.org/10.1002/jgrf.20148, 2013JF002796

Kean, J. W., McGuire, L. A., Rengers, F. K., Smith, J. B., & Staley, D. M. (2016). Amplification of postwildfire peak flow by debris. *Geophysical Research Letters*, *43*, 8545–8553. https://doi.org/10.1002/2016GL069661

Kean, J. W., Smith, J. B., Rengers, F. K., McGuire, L. A., & Staley, D. M. (2019). wildfire debris-flow monitoring data, Las Lomas, 2016 Fish Fire, Los Angeles County, California, November 2016 to February 2017, U.S. Geological Survey data release. https://doi.org/10.5066/P9F3YTBP

Kean, J. W., Staley, D. M., & Cannon, S. H. (2011). In situ measurements of post-fire debris flows in Southern California: Comparisons of the timing and magnitude of 24 debris-flow events with rainfall and soil moisture conditions. *Journal of Geophysical Research*, *116*, F04019. https://doi.org/10.1029/2011JF002005

Kean, J. W., Staley, D. M., Leeper, R. J., Schmidt, K. M., & Gartner, J. E. (2012). A low-cost method to measure the timing of postfire flash floods and debris flows relative to rainfall. *Water Resources Research*, *48*, W05516. https://doi.org/10.1029/2011WR011460

Lamb, M. P., Dietrich, W. E., & Venditti, J. G. (2008). Is the critical shields stress for incipient sediment motion dependent on channel-bed slope? *Journal of Geophysical Research*, *113*, F02008. https:://doi.org/10.1029/2007JF000831

Ma, C., Wang, Y., Hu, K., Du, C., & Yang, W. (2017). Rainfall intensity-duration threshold and erosion competence of debris flows in four areas affected by the 2008 Wenchuan earthquake. *Geomorphology*, *282*, 85–95. https://doi.org/10.1016/j.geomorph.2017.01.012

Marra, F., Nikolopoulos, E. I., Creutin, J. D., & Borga, M. (2016). Space-time organization of debris flows-triggering rainfall and its effect on the identification of the rainfall threshold relationship. *Journal of Hydrology*, *541*, 246–255. https://doi.org/10.1016/j.jhydrol.2015.10.010

McGuire, L. A., Kean, J. W., Staley, D. M., Rengers, F. K., & Wasklewicz, T. A. (2016). Constraining the relative importance of raindrop- and flow-driven sediment transport mechanisms in postwildfire environments and implications for recovery time scales. *Journal of Geophysical Research: Earth Surface*, *121*, 2211–2237. https://doi.org/10.1002/2016JF003867

McGuire, L. A., & Rengers, F. K. (2019). Las Lomas hillside lidar, U.S. Geological Survey data release. https://doi.org/10.5066/P92HVD2T

McGuire, L. A., Rengers, F. K., Kean, J. W., & Staley, D. M. (2017). Debris flow initiation by runoff in a recently burned basin: Is grain-by-grain sediment bulking or en masse failure to blame? *Geophysical Research Letters*, *44*, 7310–7319. https://doi.org/10.1002/2017GL074243

Moody, J. A., Ebel, B. A., Nyman, P., Martin, D. A., Stoof, C., & McKinley, R. (2016). Relations between soil hydraulic properties and burn severity. *International Journal of Wildland Fire*, *25*(3), 279–293.

Moody, J. A., Shakesby, R. A., Robichaud, P. R., Cannon, S. H., & Martin, D. A. (2013). Current research issues related to post-wildfire runoff and erosion processes. *Earth-Science Reviews*, *122*, 10–37. https://doi.org/10.1016/j.earscirev.2013.03.004

Nyman, P., Sheridan, G. J., Smith, H. G., & Lane, P. N. J. (2014). Modeling the effects of surface storage, macropore flow and water repellency on infiltration after wildfire. *Journal of Hydrology*, *513*, 301–313. https://doi.org/10.1016/j.jhydrol.2014.02.044

Oakley, N. S., Lancaster, J. T., Kaplan, M. L., & Ralph, F. M. (2017). Synoptic conditions associated with cool season post-fire debris flows in the Transverse Ranges of Southern California. *Natural Hazards*, *88*(1), 327–354. https://doi.org/10.1007/s11069-017-2867-6

Palucis, M. C., Ulizio, T., Fuller, B., & Lamb, M. P. (2018). Intense granular sheetflow in steep streams. *Geophysical Research Letters*, *45*, 5509–5517. https://doi.org/10.1029/2018GL077526

Parker, G., Klingeman, P. C., & McLean, D. G. (1982). Bedload and size distribution in paved gravel-bed streams. *Journal of Hydraulic Engineering*, *108*(HY4), 544–571.

Prancevic, J. P., Lamb, M. P., & Fuller, B. M. (2014). Incipient sediment motion across the river to debris-flow transition. *Geology*, *42*(3), 191. https://doi.org/10.1130/G34927.1

Rengers, F. K., McGuire, L. A., Kean, J. W., Staley, D. M., & Hobley, D. E. J. (2016). Model simulations of flood and debris flow timing in steep catchments after wildfire. *Water Resources Research*, *52*, 6041–6061. https://doi.org/10.1002/2015WR018176

Staley, M. D., Gartner, E. J., & Kean, W. J. (2015). Objective definition of rainfall intensity-duration thresholds for post-fire flash floods and debris flows in the area burned by the Waldo Canyon Fire, Colorado, USA, *Engineering geology for society and territory* (vol. 2, pp. 621–624). Cham: Springer International Publishing.

Staley, D. M., Kean, J. W., Cannon, S. H., Schmidt, K. M., & Laber, J. L. (2013). Objective definition of rainfall intensity–duration thresholds for the initiation of post-fire debris flows in Southern California. *Landslides*, *10*(5), 547–562. https://doi.org/10.1007/s10346-012-0341-9

Staley, D. M., Negri, J. A., Kean, J. W., Laber, J. L., Tillery, A. C., & Youberg, A. M. (2017). Prediction of spatially explicit rainfall intensity-duration thresholds for post-fire debris-flow generation in the western United States. *Geomorphology*, *278*, 149–162. https://doi.org/10.1016/j.geomorph.2016.10.019

Staley, D. M., Wasklewicz, T. A., & Kean, J. W. (2014). Characterizing the primary material sources and dominant erosional processes for post-fire debris-flow initiation in a headwater basin using multi-temporal terrestrial laser scanning data. *Geomorphology*, *214*, 324–338. https://doi.org/10.1016/j.geomorph.2014.02.015

Stoof, C. R., Vervoort, R. W., Iwema, J., van den Elsen, E., Ferreira, A. J. D., & Ritsema, C. J. (2012). Hydrological response of a small catchment burned by experimental fire. *Hydrology and Earth System Sciences*, *16*(2), 267–285. https://doi.org/10.5194/hess-16-267-2012

Suwa, H., Okano, K., & Kanno, T. (2009). Behavior of debris flows monitored on test slopes of Kamikamihorizawa Creek, Mount Yakedake, Japan. *International Journal of Erosion Control Engineering*, *2*(2), 33–45. https://doi.org/10.13101/ijece.2.33

Takahashi, T. (1978). Mechanical characteristics of debris flow. *Journal of the Hydraulics Division*, *104*(8), 1153–1169.

Tang, H., McGuire, L. A., Rengers, F. K., Kean, J. W., Staley, D. M., & Smith, J. B. (2019). Evolution of debris-flow initiation mechanisms and sediment sources during a sequence of postwildfire rainstorms. *Journal of Geophysical Research: Earth Surface*, *124*, 1572–1595. https://doi.org/10.1029/2018JF004837

Tognacca, C., Bezzola, G., & Minor, H. (2000). Threshold criterion for debris-flow initiation due to channel-bed failure. In *Proc. of the 2nd int. conf. on debris flow, hazards and mitigation, taipei/taiwan (wieczorek, gf, ed.). aa balkema* (pp. 89–97). Rotterdam.